Welding in the World
https://doi.org/10.1007/s40194-020-00987-z

RESEARCH PAPER

Development of shielded metal arc welding electrodes to achieve carbide-free bainitic weld microstructures

Sudharsanan Sundaram[1] · G. D. Janaki Ram[2] · Murugaiyan Amirthalingam[1]

Received: 28 July 2020 / Revised: 1 September 2020 / Accepted: 2 September 2020

Abstract

Carbide-free bainite (CFB) microstructures containing a mixture of nano-sized retained austenite laths and bainitic ferrite exhibit a good combination of strength, ductility, and toughness. In this work, an attempt was made to identify welding electrode compositions with a carbon content of about 0.35 to 0.5 wt.% to achieve carbide-free bainite microstructures in multi-pass shielded metal arc welds. Suitable alloy compositions were designed using a commercial neural network–based database, considering thermodynamic parameters such as allotropic phase boundary (X_{To}), $\Delta G^{\gamma-\alpha}$ (driving force for transformation) and martensite start temperatures. Three different alloy compositions were identified using this approach. Shielded metal arc welding (SMAW) electrodes were fabricated with the compositions identified and the samples extracted from the weld deposits were used for dilatometer studies, metallurgical characterisation, and mechanical property evaluation. Based on the results, an optimised electrode composition and welding parameters were identified to stabilise the carbide-free bainitic microstructures in weld metal.

Keywords Carbide-free bainite · SMAW electrode · Weld microstructure

1 Introduction

Steel microstructures containing bainitic ferrite and nano-sized retained austenite laths are known to offer a good combination of tensile strength (up to 1.8 GPa), total elongation (up to 30%), and toughness up to 40 MPa $m^{1/2}$ [1]. These high-strength steels are currently considered candidate materials for balliest resistance armour tank bodies, construction of heavy-duty cranes, and load bearing members in earthmovers. This combination of properties is achieved by the presence of fine bainitic ferrite plates and filmy inter-lath retained austenite. This microstructure is stabilised by suppressing nucleation of cementite while austenite is transforming to bainite [1, 2]. The suppression of cementite during the transformation of austenite to bainite is possible by the addition of silicon (about 1.5 wt.% or higher) [3–5].

Carbide-free bainitic (CFB) microstructures are also known to provide adequate resistance against hydrogen-assisted cold cracking [6, 7]. The retained austenite present in CFB structure delays hydrogen-assisted cold cracking in three ways: (i) dissolving atomic hydrogen in the austenite matrix, as the solubility of hydrogen is more in austenite than in ferrite/martensite; (ii) trapping the atomic hydrogen in the austenite matrix, as the diffusivity of hydrogen is low in austenite; and (iii) trapping atomic hydrogen in the austenite/ferrite interphase lath boundaries [6]. CFB microstructures can be considered a safe weld microstructure for high-strength steels with a carbon content of ranging from 0.35 to 0.5 wt.%. Careful control of welding procedures is however required to stabilise the CFB.

High-strength steel welds are susceptible to hydrogen-assisted cold cracking (HACC) due to the presence of diffusible hydrogen, high residual stresses, and hard microstructure in the weld metals. Therefore, for welding high-strength steels, under-matching austenitic stainless steel electrodes are widely used to prevent HACC [8, 9]. By establishing

Recommended for publication by Commission II - Arc Welding and Filler Metals

✉ Sudharsanan Sundaram
sudharmet@gmail.com

G. D. Janaki Ram
jram@msme.iith.ac.in

Murugaiyan Amirthalingam
murugaiyan@iitm.ac.in

[1] Indian Institute of Technology Madras, Chennai, TN, India

[2] Indian Institute of Technology Hyderabad, Yeddumailaram, TS, India

Published online: 07 October 2020

welding procedures to stabilise carbide-free bainitic microstructures in high-strength steel weld metals, the need for expensive and low -strength austenitic stainless steel electrodes can be avoided.

Carbide-free bainitic microstructures can be achieved in weld metals by proper design of electrode composition and selection of appropriate welding procedures. Bhadesia and his co-workers designed welding electrode with a composition of 0.1C-2Mn0.8-1Si (wt.%). Multi-pass 20-mm-thick weld metals were made as per ISO 2560 without preheating and post weld heat treatments. The weld microstructure contained carbide-free bainite along with undesirable blocky retained austenite and martensite [10]. Fang et al. adopted a regeneration method to produce a weld metal with the same microstructure as the base metal during autogenous welding of CFB steel plate. With post weld isothermal holding in between bainite start (B_S) and martensite start (M_S) temperatures, the desired CFB weld microstructure was obtained. The mechanical properties of the welds were found to be the same as base metal [11].

Krishnamurthy et al. welded armour grade quenched and tempered steel using an electrode with a composition designed to achieve carbide-free bainite in weldments. Welding was carried out with preheat of 350 °C and post weld isothermal holding at the same temperature for 6 h. It was reported that carbide-free bainite weldment demonstrated better weld joint efficiency than austenitic weld joints; however, the presence of undesirable blocky retained austenite affected the toughness of the weldments [12].

In the current study, welding electrode compositions were designed and welding procedures were developed with appropriate preheating and post weld isothermal holding to achieve a carbide-free bainitic microstructure in the weld metal with a carbon content of about 0.35–0.5 wt.%. The preheating and interpass temperatures were set above M_S temperature so that during welding, the weld metal temperature does not fall below M_S temperature. Post weld isothermal holding is carried out at an appropriate temperature and time to (i) ensure the completion of carbide-free bainitic transformation in the weld metal, (ii) avoid the retention of blocky austenite, and (iii) avoid the formation of martensite upon cooling to room temperature.

The main objectives in designing the electrode composition and deriving suitable welding procedures are to obtain:

- *Weld microstructure*: nano-sized inter-lath austenite of about 15–20 vol.% in a carbide-free bainite matrix. The percolation threshold of retained austenite in carbide-free bainitic microstructure is 10 vol.%; below this threshold limit, retained austenite is geometrically isolated. High strength and toughness can be achieved when austenite exists as a continuous network at the inter-lath bainitic ferrite boundaries in the microstructure [13, 14]. Therefore, it is aimed to achieve a CFB microstructures with 15–20 vol.% inter-lath retained austenite.
- *Martensite start (M_S) temperature below 300 °C*: The lowest bainitic transformation temperature is determined by the M_S temperature of the alloy. The lath size of bainite and volume fraction of blocky austenite decreases with a decrease in transformation temperatures. M_S temperature increases significantly with a decrease in carbon concentration [3, 15]. A carbon content of about 0.35 to 0.5 wt.% is considered to be desirable to obtain an M_S temperature below 300 °C and to accelerate the kinetics of bainite formation.
- *Transformation time (post weld isothermal holding time)*: Post weld isothermal holding time after welding should be in a realistic duration to facilitate the completion of bainitic transformation. It is also one of the major requirements for commercialising the welding procedures. In earlier studies, it was reported that post weld isothermal holding for 5 days was required to complete the bainitic transformation [11]. In this work, it is aimed to achieve the required CFB microstructures with a post weld isothermal holding for about 5 h.
- *Mechanical properties of the weld metals*: The major applications of these electrodes are to weld high-strength steels with a tensile strength of 1 GPa or more. The proposed electrodes are an alternative for under matching stainless steel electrodes. The strength of CFB microstructure depends on the lath size of bainite [14] and the refinement of the microstructures is largely depending on the carbon content [3, 15]. With carbon content ranging from 0.35 to 0.5 wt.%, it is aimed to achieve all weld ultimate strengths of about 1.5 GPa.

2 Design of electrode chemistry

In the design of carbide-free bainite microstructures, various alloying elements are added for specific purposes. Additions of aluminium and cobalt improve the kinetics of banitic transformation [16]. Nickel additions increase toughness and strength without affecting ductility [4]. Manganese and chromium are added for hardenability [15, 17]. Molybdenum addition of up to 0.25 wt.% is known to avoid temper embrittlement arising from phosphorus and it also improves hardenability [4]. Silicon addition of 1.5 wt.% suppresses cementite formation. The addition of carbon (i) significantly lowers the martensite start temperature, (ii) decreases the maximum attainable volume fraction of bainitic ferrite, and (iii) leads to an increase in cold cracking susceptibility [12]. In this work, the base composition of the welds is targeted to contain a

Table 1 Designed alloy compositions

Elements wt.%	C	Si	Mn	Ni	Mo	Cr
Alloy A	0.35	1.5	1.5	2.0	0.25	–
Alloy B	0.38	1.5	1.5	0.5	0.25	2.5
Alloy C	0.45	1.5	1.0	0.5	0.25	3.5

carbon concentration ranging from 0.35 to 0.5 wt.%, silicon with a minimum of 1.5 wt.% and appropriate additions of elements such as Mn, Ni, Cr, Mo, Al, and Co.

A commercial neural network–based database JMatPro™ was used to construct TTT diagrams for various compositions. Martensite start temperature (M_S), bainite start temperature (B_S), the kinetics of transformation under various isothermal holding temperatures, and the critical cooling rates to avoid intermediate phase transformations were identified as key parameters in the TTT diagrams. The alloy additions were varied individually to study its influence on these key parameters. It is observed that manganese and nickel improve hardenability and decrease the transformation kinetics. Nickel and manganese lower M_S temperature. Chromium improves hardenability but significantly decreases the transformation kinetics. Cobalt and silicon show no effect on hardenability or transformation kinetics. Aluminium slightly increases the transformation kinetics but reduces the hardenability significantly. Carbon significantly lowers the M_S temperature, reduces the transformation kinetics, and increases hardenability. Based on these observations, alloy A was designed and its composition is given in Table 1. The TTT diagram calculated for this composition is shown in Fig. 1.

The alloy design was also optimised using X_{To} (the allotropic phase boundary denoting the carbon concentration at which the Gibbs energies of austenite and bainitic ferrite are equal at a given temperature) calculated from the Thermocalc™ database and M_S temperature calculated using the Andrews equation [18].

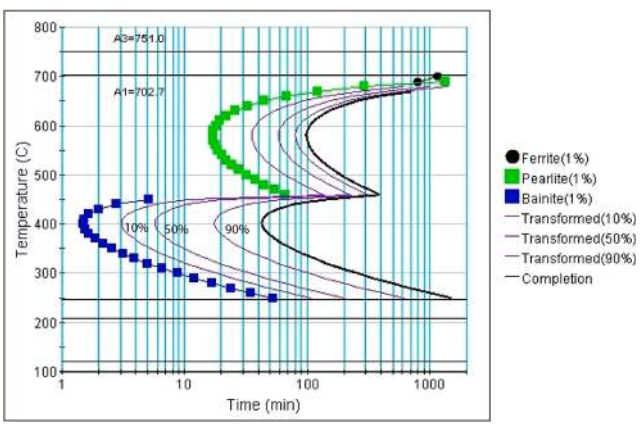

Fig. 1 TTT diagram calculated using JMatPro™ for alloy A

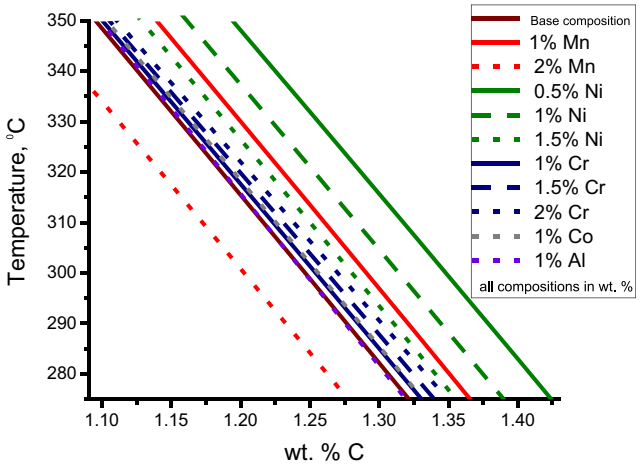

Fig. 2 Variation of X_{To} as a function of alloying elements. Base composition: 0.35C-1.5Si-1.5Mn-2Ni-0.5Cr-0.25Mo-0.5Al-0.5Co (wt.%)

Alloy A was taken as a reference and a base composition of 0.35C-1.5Si-1.5Mn-2Ni-0.5Cr-0.25Mo-0.5Al-0.5Co (wt.%) was selected. This base composition was further optimised to enable maximum X_{To} at a given isothermal holding temperature. The X_{To} value of base composition was calculated using Thermocalc™ database (TCFE9); subsequently, each element was varied independently with a range of 0.5 wt.% and its influence on X_{To} was studied. The variation of X_{To} as a function of elemental compositions is shown in Fig. 2.

It can be seen from Fig. 2 that an increase in manganese and nickel significantly shifts X_{To} towards lower carbon concentration. An increase in chromium and cobalt shifts X_{To} towards higher carbon concentration. An increase in aluminium has no effect on X_{To}.

Alloy B was designed using this approach and the optimised composition is given in Table 1. Nickel was reduced to 0.5 wt.% due to its influence on X_{To} compared with the selected base composition. As manganese shifts X_{To} towards lower carbon concentration, it was kept 1.5 wt.% as it significantly lowers M_S temperature. Though both chromium and cobalt shift X_{To} towards higher carbon concentration, an increase in cobalt concentration shifts M_S temperature towards higher temperature and therefore, only chromium was added to the base composition. As aluminium has no effect on both X_{To} and M_S temperature, it was not considered in alloy B. The M_S temperature of the designed alloy composition B calculated using the Andrews equation was 280 °C.

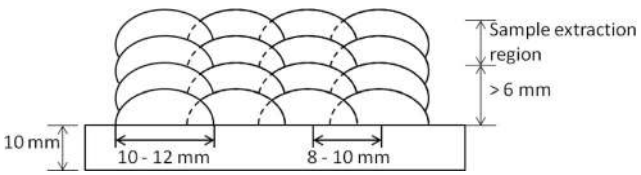

Fig. 3 Schematic of the deposited SMA weld metal

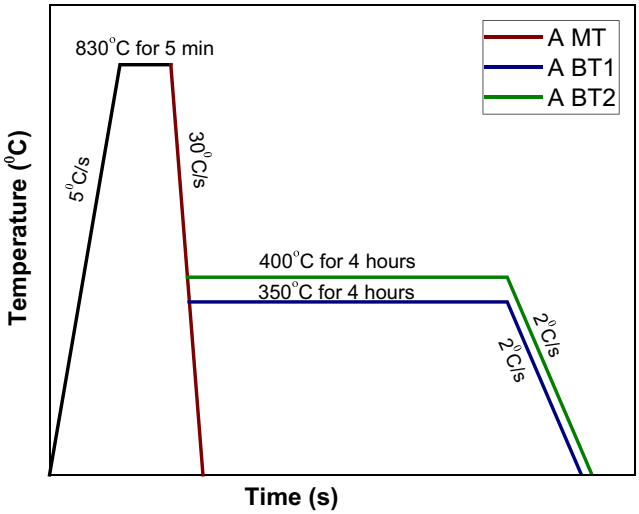

Fig. 4 Thermal cycle used for dilatometry analysis in alloy A, martensitic transformation (A MT), bainitic transformation 1 (A BT1), bainitic transformation 2 (A BT2)

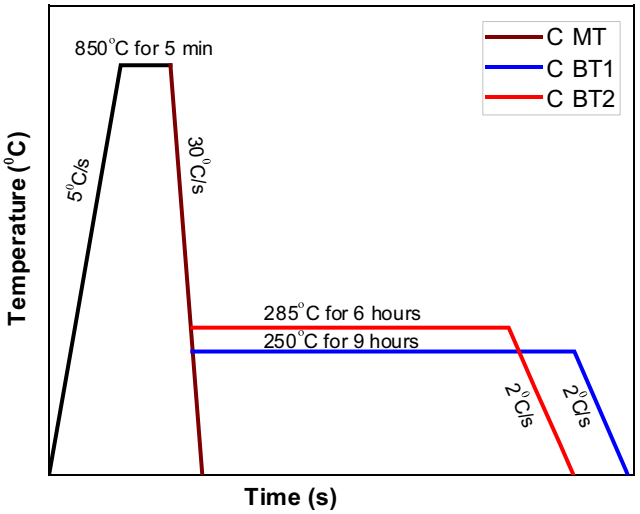

Fig. 6 Thermal cycle used for dilatometry analysis in alloy C, martensitic transformation (C MT), bainitic transformation 1 (C BT1), bainitic transformation 2 (C BT2)

For alloy C, the composition was identified using X_{To} as well as the Gibbs energy difference between bainitic ferrite and austenite, $\Delta G^{\gamma-\alpha}$ (driving force for transformation) calculated from a Thermocalc™ database (TCFE9). An increase in carbon significantly reduces the driving force. Manganese, nickel, and chromium decrease the driving force in the order of Mn > Ni > Cr. In alloy C, manganese was reduced by 0.5 wt.% as it decreases driving force as well as shifts X_{To} to lower carbon content. Chromium in alloy C was increased by about 1 wt.% as it shifts X_{To} to a higher carbon content and its influence on driving force was minimal. In order to decrease M_S further below than in alloy B, an attempt was made to increase carbon content by 0.07 wt.%. The M_S temperature of the designed alloy composition C calculated using the Andrews equation is 254 °C.

3 Experimental details

Shielded metal arc welding (SMAW) electrodes were fabricated for the identified compositions. SMAW electrodes were made using a 4-mm-diameter low carbon steel core wire covered with rutile type flux. All the alloying elements necessary to achieve desired weld compositions were added via the flux, and welding trials were carried out.

Using the developed electrodes, weld deposition was made by depositing four layers, each layer having four passes on a low carbon steel base plate. The schematic of the deposited weld metal is shown in Fig. 3. The welding trials were carried out with a preheating temperature of 300 °C. An electrical resistance heater was used to achieve the desired preheat and a K type thermocouple was welded on to the base plate prior to

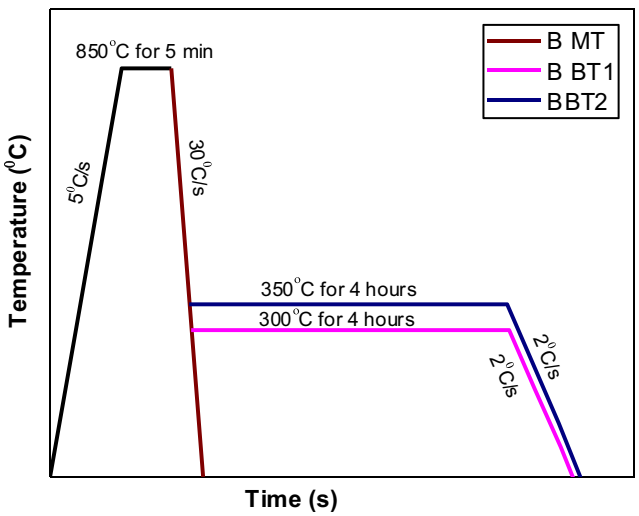

Fig. 5 Thermal cycle used for dilatometry analysis in alloy B, martensitic transformation (B MT), bainitic transformation 1 (B BT1), bainitic transformation 2 (B BT2)

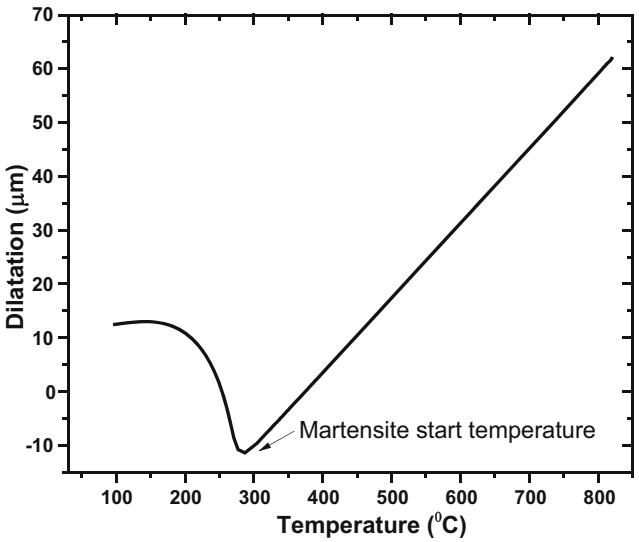

Fig. 7 Dilatation behaviour of alloy A, A MT thermal cycle revealing M_S temperature, while cooling from 830 °C

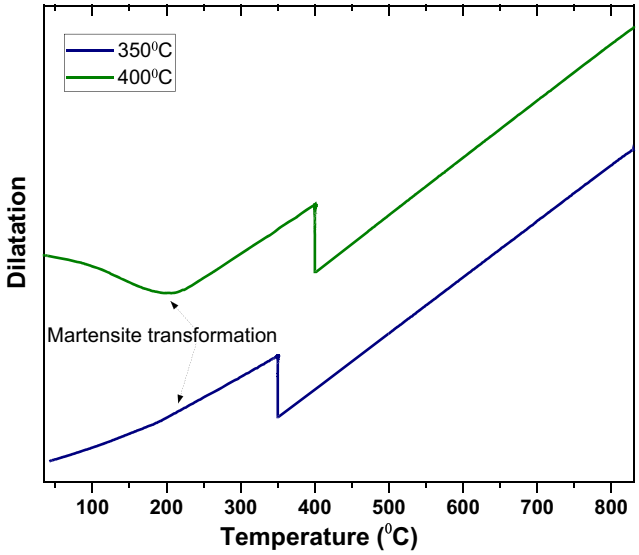

Fig. 8 Dilatation behaviour as a function temperature for alloy A, A BT1 (350 °C) and A BT2 (400 °C) thermal cycles, while cooling from 830 °C

welding to control the preheating. After welding, the weld coupons were immediately transferred to muffle furnace maintained at 300 °C. The weld coupons were kept in the furnace for 4 h and subsequently cooled in air to room temperature. The preheating and post heating were carried to avoid the formation of brittle martensite in the weld metal.

The welding trials were primarily carried out to extract samples to analyse weld metal composition and for the dilatometry analysis to subsequently optimise welding procedures for a given composition. Samples were extracted at 6 mm above the base plate in the weld deposit to avoid possible dilution from the substrate. The weld metal compositions were determined using a Spectra™ optical emission spectroscopy (OES) and Bruker G4 ICARUS HF™ C-S analyser.

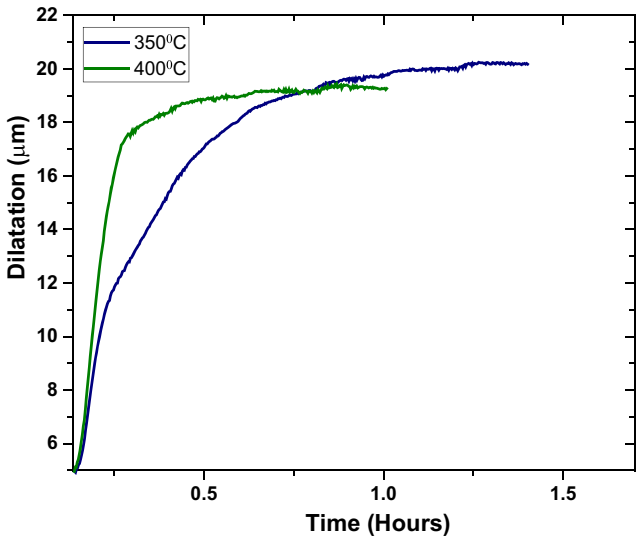

Fig. 9 Dilatation behaviour as a function of holding time for alloy A, A BT1 (350 °C) and A BT2 (400 °C) thermal cycles

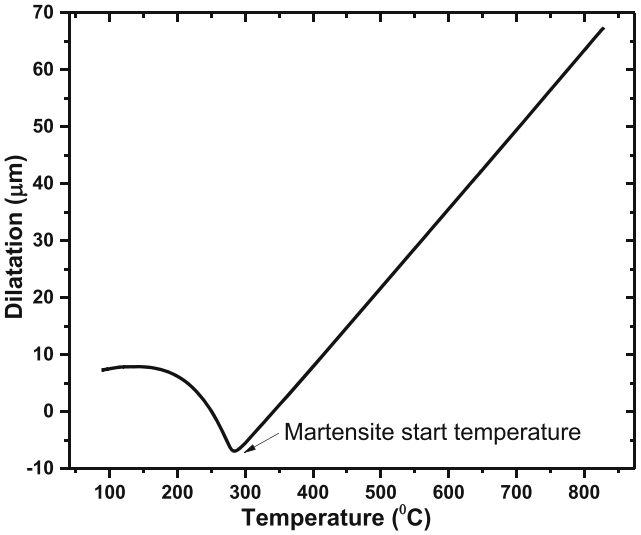

Fig. 10 Dilatation behaviour of alloy B, B MT thermal cycle revealing M_S temperature, while cooling from 850 °C

Dilatometry analysis was carried out to identify suitable post weld isothermal holding time and temperature required to stabilise a carbide-free bainite microstructure in the weld metal. Dilatometer experiments were carried out in a Gleeble™ 3800 thermomechanical simulator. Cylindrical samples of 6 mm diameter and 85 mm in length obtained from SMAW deposits were used for these studies. A K type thermocouple was welded on the surface at the centre of the samples and was used to control the temperature. The thermal cycles of the Gleeble™ dilatometry studies for alloys A, B, and C are given in Figs. 4, 5, and 6, respectively. The samples used for Gleeble™ dilatometer studies were subsequently cross-sectioned at thermocouple location for metallurgical characterisation. It should be noted that among a number of

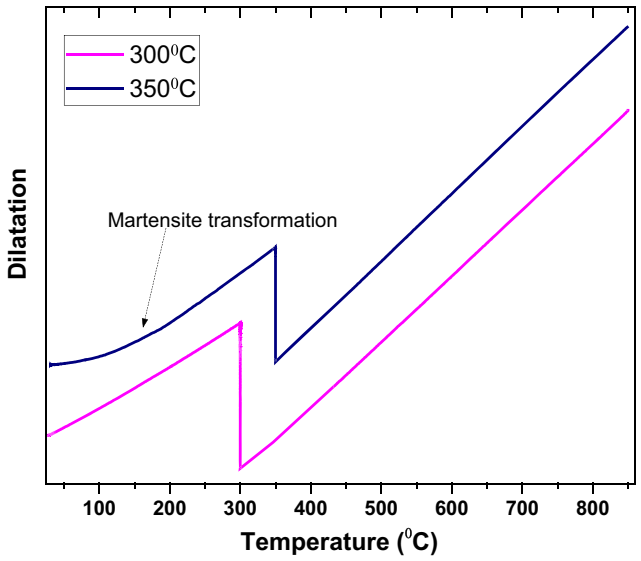

Fig. 11 Dilatation behaviour with temperature of alloy B, B BT1 (300 °C), B BT2 (350 °C) thermal cycles, while cooling from 850 °C (*note*: no martensite transformation observed for B BT1 thermal cycle)

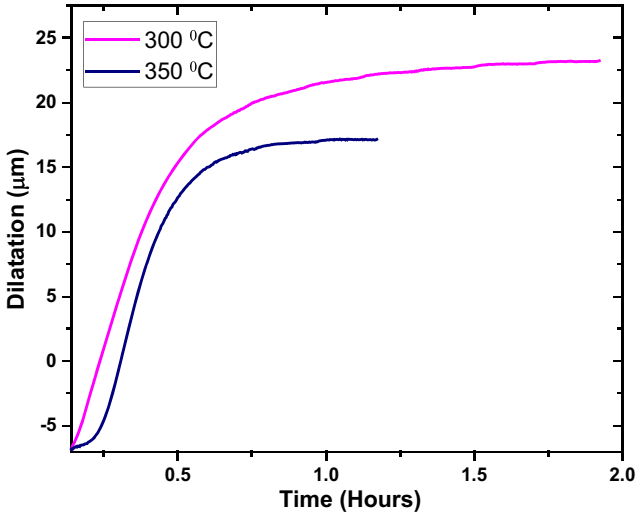

Fig. 12 Dilatation behaviour as a function of holding time for alloy B, B BT1 (300 °C) and B BT2 (350 °C) thermal cycles

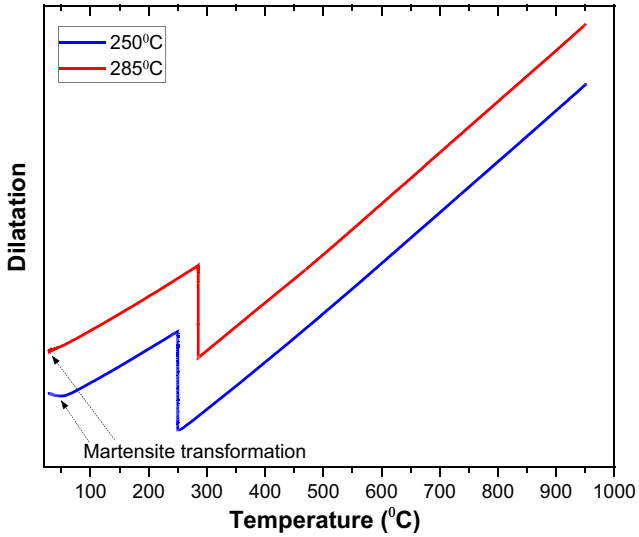

Fig. 14 Dilatation behaviour as a function of temperature of alloy C, C BT1 (250 °C), C BT2 (285 °C) thermal cycles, while cooling from 850 °C

thermal cycles used for the dilatometry analysis, two optimal thermal cycles per sample are presented here for metallurgical comparison and analysis.

For optical microscopy observations, samples were metallographically polished and etched with 2 vol.% Nital and Klemms I reagent. For scanning electron microscopy, samples were etched with 2 vol.% Nital and analysis was carried out on a FEI Quanta 400 equipment.

Retained austenite measurements were carried out on the dilatometry samples. Retained austenite was measured using a ProtoIXRD™ retained austenite measurement system. Retained austenite was calculated from the integrated intensities of (200), (220) peaks of austenite and (200), (211) peaks of ferrite.

After analysing the phase transformation behaviour from dilatometry analysis, quantification of retained austenite and microscopy analysis, suitable post weld isothermal holding temperature, and time for each composition were identified. Subsequently, SMA welding was carried out using the optimised post weld isothermal holding procedures identified from Gleeble™ dilatometry studies. Welds produced from optimised welding procedures were further characterised using transmission electron microscopy. Mechanical properties of the weld metals were analysed using compression testing. Transmission electron microscopy (TEM) analysis and compression tests were carried out on the samples extracted from the weld metals. Compression tests were carried out in Gleeble™ 3800 thermomechanical simulator. For TEM analysis, a thin foil of thickness 80–90 µm was prepared and 3-mm-diameter circular

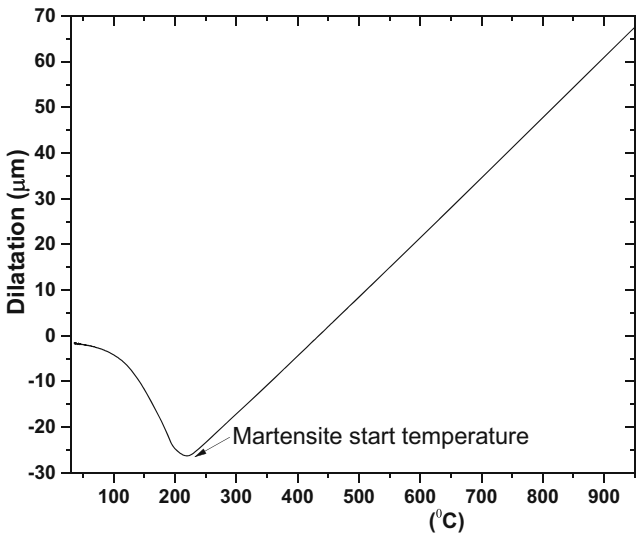

Fig. 13 Dilatation behaviour of alloy C, C MT thermal cycle revealing M_S temperature, while cooling from 850 °C

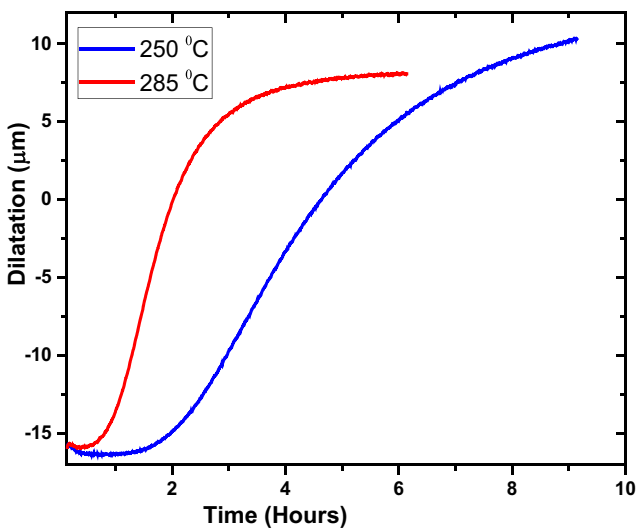

Fig. 15 Dilatation behaviour with time of alloy C, C BT1 (250 °C), C BT2 (285 °C) thermal cycles

Table 2 Chemical composition of weld metals

Elements wt.%	C	Si	Mn	Ni	Mo	Cr
Alloy A	0.35	1.36	1.90	1.99	0.20	0.03
Alloy B	0.375	1.53	1.63	0.17	0.19	2.23
Alloy C	0.53	1.93	0.96	0.34	0.21	4.23

discs were punched out. Perforation at the centre of the disc was done by electropolishing on twin jet polisher at 15 V for 10 s in a solution consisting of 10 vol.% perchloric acid and 90 vol.% acetic acid at room temperature. The samples were examined on Tecnai T20™ equipment with an accelerating voltage of 200 keV in bright field imaging mode.

4 Results

The weld metal compositions determined using OES analysis are given in Table 2. It is observed that the carbon and chromium concentrations of alloy C welds are notably different than the designed alloy C composition shown in Table 1.

Transformation characteristics were studied using dilatometry analysis. The martensite start temperature of alloy A is determined from the dilatation behaviour of alloy A MT thermal cycle and is shown in Fig. 7. The M_S temperature of alloy A is 295 °C. The dilatation behaviour of alloy A during isothermal holding at 350 °C and 400 °C is determined and shown in Fig. 8. Martensite formation was observed in both thermal cycles upon cooling from the isothermal holding temperature. The austenite transformation kinetics determined from dilatation behaviour for A BT1 and A BT2 thermal cycles is shown in Fig. 9. The bainite formation approaches saturation at approximately 1 h and 15 min for A BT1 and 50 min for A BT2 samples.

Table 3 Bainite formation saturation time for various thermal cycles

Thermal cycle	Isothermal holding temperature, °C	Bainite formation saturation time
A BT1	350	1 h 15 min
A BT2	400	50 min
B BT1	300	1 h 45 min
B BT2	350	1 h
C BT1	250	9 h
C BT2	285	5 h 40 min

The martensite start temperature of alloy B determined from the dilatation behaviour of alloy B MT thermal cycle and is shown in Fig. 10. The M_S temperature of alloy B is 290 °C and observed to be about 10 °C higher than that calculated using the Andrews equation. The dilatation behaviour with temperature for alloy B during isothermal holding at 300 °C and 350 °C is shown in Fig. 11. It is observed that there is no martensite transformation during cooling from isothermal holding temperature for the B BT1 thermal cycle, whereas martensite transformation is observed for the B BT2 thermal cycle. The transformation kinetics of alloy B during isothermal holding at 300 and 350 °C are shown in Fig. 12. The bainite formation approaches saturation at approximately 1 h and 45 min for B BT1 and 1 h for B BT2 thermal cycles.

The martensite start temperature of alloy C determined from the dilatometry analysis of C MT thermal cycle and shown in Fig. 13. The M_S temperature of alloy C is 235 °C. Dilatation behaviour as a function temperature for alloy C is shown in Fig. 14. Martensite transformation is observed upon cooling from isothermal holding temperatures (250 and 285 °C) in both C BT1 and C BT2 thermal cycles.

The transformation kinetics of alloy C during isothermal holding at 250 and 285 °C are determined from dilatation behaviour of C BT1 and C BT2 thermal cycles and are shown in Fig. 15. The bainitic transformation approaches saturation approximately after 9 h for C BT1 and 5 h and 40 min for C BT2 thermal cycles. The bainite formation saturation time for all alloy compositions is consolidated and given in Table 3.

The microstructures of alloy A samples subjected to A BT1 (isothermal holding 350 °C) and A BT2 (isothermal holding 400 °C) thermal cycles are given in Fig. 16. The amount of blocky retained austenite constituents is more in A BT2

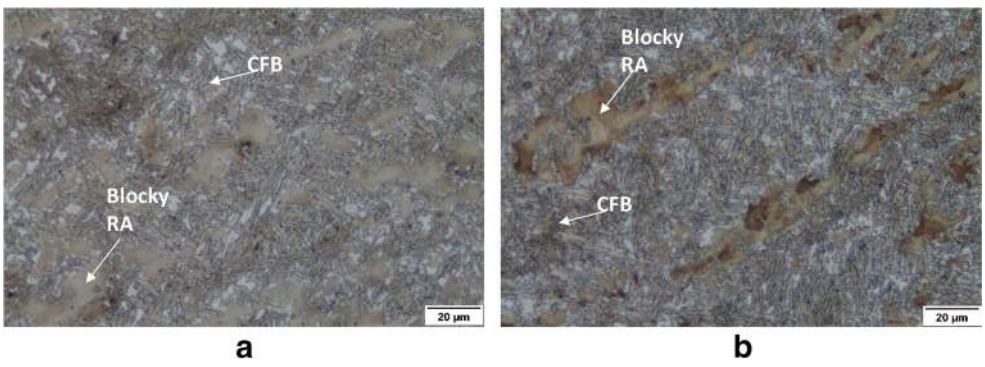

Fig. 16 Micrographs of alloy A BT1 (**a**) and alloy A BT2 (**b**) thermal cycles. RA, retained austenite; CFB, carbide-free bainite

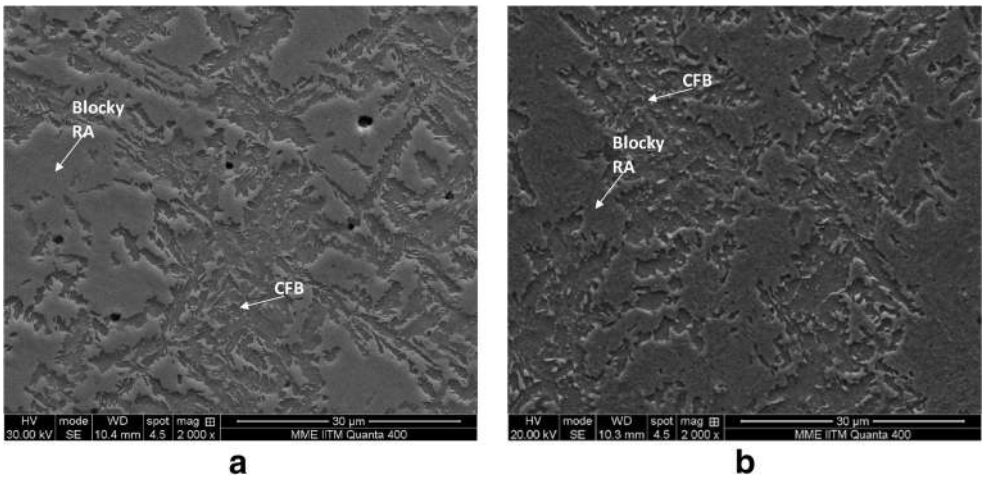

Fig. 17 SE images of alloy A BT1 (**a**) and alloy A BT2 (**b**) thermal cycles

compared with that in A BT1. This is also evident in SE images given in Fig. 17.

The microstructures of alloy B samples subjected to B BT1 (isothermal holding 300 °C) thermal cycle are shown in Fig. 18. The microstructure contains CFB and blocky retained austenite. The amount of RA constituents is found to be lower than that of alloy A. The same can also be observed in SE images of B BT1 and B BT2 in Fig. 19.

The SE images of alloy C samples subjected to C BT1 and C BT2 thermal cycles are shown in Fig. 20. It contains both CFB and blocky retained austenite constituents. It is observed that the amount of retained austenite (RA) constituent is higher than that of alloy B samples and lesser than that of alloy A samples. It is also observed that in each alloy composition, samples at higher isothermal holding temperature show more RA constituent than the sample at lower isothermal holding temperature.

The retained austenites measured using XRD for alloy A, alloy B, and alloy C of Gleeble™-tested samples with various thermal cycles are given in Table 4.

Based on these observations, further welding trials were carried out for three electrode compositions using post weld isothermal holding at 350 °C (A BT1), 300 °C (B BT1), and 285 °C (C BT2) for alloys A, B, and C respectively.

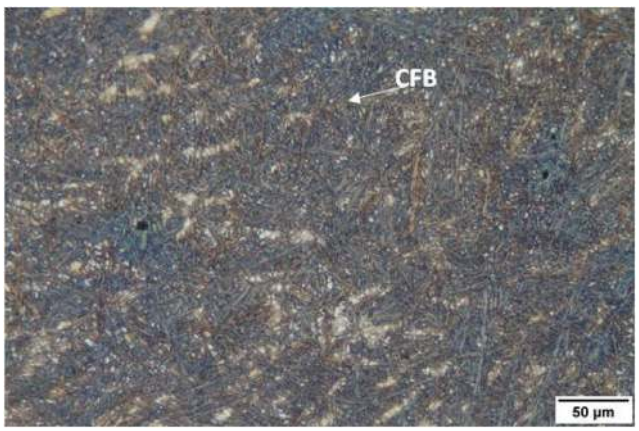

Fig. 18 Micrograph of B BT1 thermal cycle

The compression behaviour of samples extracted from A BT1, B BT1, and C BT2 welds are shown in Fig. 21. It is observed that C BT2 weld shows higher strength than other welds. B BT1 weld shows uniform plastic deformation (total elongation) before failure.

The TEM images of A BT1, B BT1, and C BT2 welds are shown in Fig. 22. The presence of lamellar structure of bainitic ferrite (BF) and filmy austenite (FA) was observed in all welds. The bainitic ferrite lath size is smaller in C BT2 welds compared with that in other welds.

5 Discussions

The weld compositions determined using OES analysis are similar to the designed composition except for alloy C. The carbon and chromium concentrations of alloy C welds are notably different from the designed composition. The addition of carbon significantly lowers the M_S temperature; the M_S temperature of alloy C is considerably lower than that calculated using the Andrews equation for the designed composition.

Dilatometer experiments revealed the transformation characteristics of each alloy composition. It is evident from dilatation behaviour of alloy A after isothermal holding at 350 and 400 °C (Figs. 7 and 8) that martensite also formed apart from CFB during cooling after isothermal holding. This is due to the fact that austenite retained upon the saturation of bainite formation contained lower carbon content. In this case, the carbon is not enriched enough in austenite being stabilised; this leads to the formation of martensite upon cooling from isothermal holding temperatures. This argument is also valid for similar observation of martensite transformation upon cooling from isothermal transformation in other alloy compositions. The austenite transformation kinetics of alloy C is

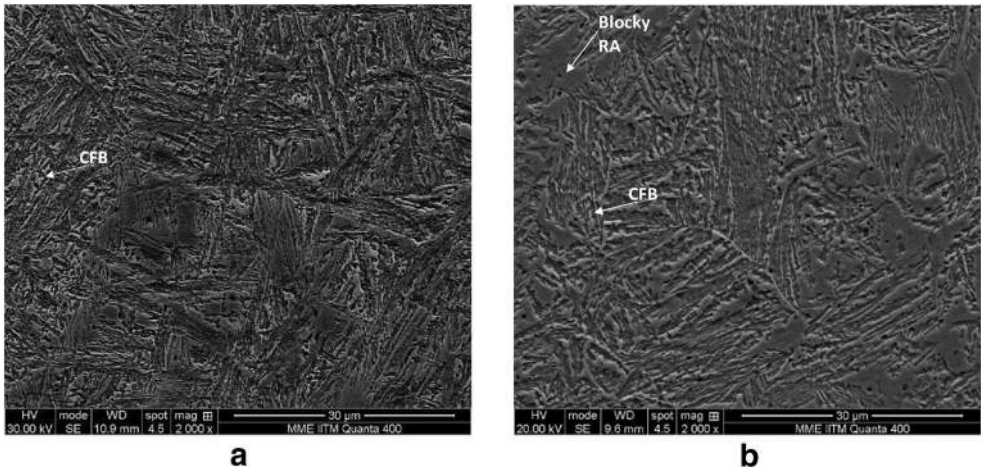

Fig. 19 SE images of B BT1 (**a**) and B BT2 (**b**) sample

found to be slower than other alloy compositions (Table 3). This is due to higher carbon concentration in alloy C which retards the transformation of austenite to low temperature products. The presence of the blocky retained austenite constituent is greater in the alloy A BT2 thermal cycle than any other sample and thermal cycles. This is due to the use of higher transformation temperature (400 °C), where CFB formation saturates quickly and results in a high volume fraction of blocky retained austenite.

The microstructure of alloy B after BT1 thermal cycle shows the lowest blocky retained austenite than of other samples. This is due to the decreased transformation temperature (300 °C) and the presence of alloying elements in alloy B shifts the X_{To} towards higher C concentration. The shift of X_{To} towards high C concentration facilitates the formation of more of CFB and less of blocky retained austenite.

Despite using low isothermal holding temperatures (250 and 280 °C) for alloy C, the volume fraction of blocky retained austenite constituents is found to be greater compared with that in other thermal cycles. This is due to the presence of high carbon concentration of alloy C (0.53 wt.%). During the isothermal holding, austenite stabilisation occurs readily upon reaching X_{To} and results in increased volume fraction of blocky austenite.

Retained austenite measured for each alloy compositions is in the order of 10 to 20 vol.%. Apart from retained austenite, the microstructures of all the samples under investigation contain carbide-free bainite and martensite except for alloy B BT1 thermal cycle. For B BT1, the volume fraction of CFB can be calculated from the measured volume fraction of retained austenite as no martensitic transformation is observed upon cooling from isothermal holding (300 °C).

From the dilation behaviour, microstructure analysis, and retained austenite measurements, the post weld isothermal holding temperatures of A BT1, B BT1, and C BT2 thermal cycles are considered to be optimal for alloys A, B, and C, respectively. These thermal cycles show high volume fraction of CFB, no or low fraction of martensite, and adequate volume fraction of retained austenite in each alloy composition.

The B BT1 weld exhibited improved mechanical properties than A BT1 and C BT3 in compression testing. Total strain until failure was found to be 0.65 in B BT1 weld, whereas A

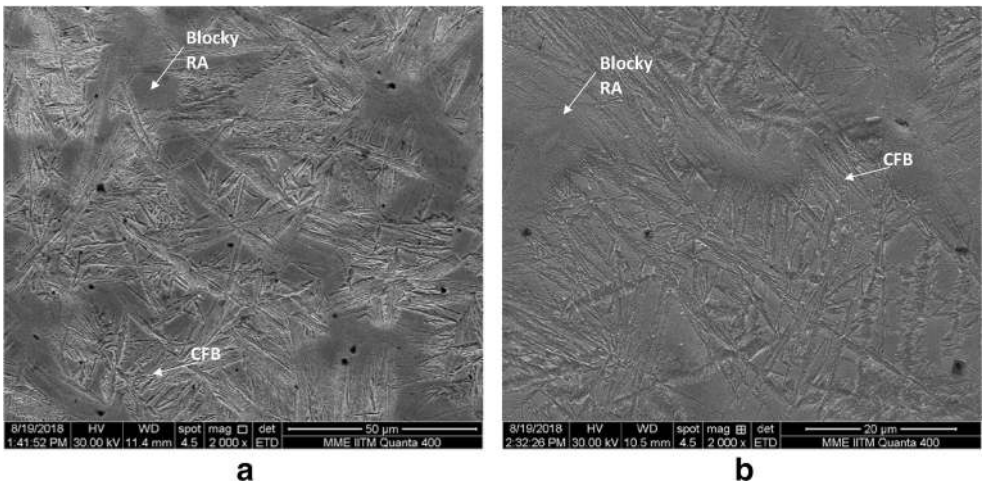

Fig. 20 SE images of C BT1 (**a**) and C BT2 (**b**) thermal cycle

Table 4 Austenite percentage measured using XRD

Thermal cycles	Austenite percentage
A BT1	11
A BT2	19
B BT1	15
B BT2	17
C BT1	17
C BT2	18

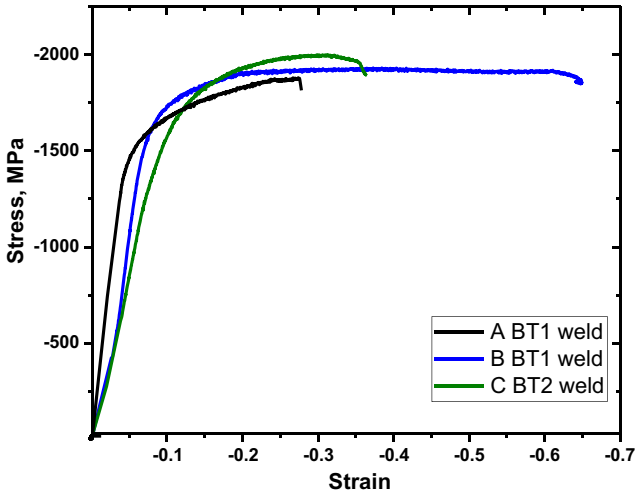

Fig. 21 Compression behaviour of A BT1, B BT1, and C BT2 welds

BT1 weld failed upon 0.28 strain and C BT3 weld failed upon 0.4 strain. The ultimate strength of B BT1 weld (1925 MPa) is slightly lower than C BT2 weld (1997 MPa) but B BT1 weld showed uniform plastic deformation behaviour before failure compared with other samples.

The lamellar structure of bainitic ferrite and filmy austenite in A BT1, B BT1, and C BT2 welds is revealed by the TEM analysis. C BT2 weld shows a finer microstructure than the other welds. The refinement of the CFB structure primarily depends on the strength of austenite at the transformation temperature [16]. An increase in carbon concentration significantly increases the strength of austenite. The increased carbon concentration in alloy C compared with that in other alloy compositions results in the CFB microstructure being refined in alloy C welds.

From these results, it can be concluded that the B BT1 cycle of alloy B is best suitable to achieve carbide-free bainitic welds with required mechanical properties. In the B BT1 thermal cycle, carbide-free bainitic microstructures can be achieved with 0.85 volume fraction of bainitic ferrite and remaining retained austenite (RA). No martensite transformation upon cooling from holding temperature is observed. Alloy B with BT1 post weld isothermal holding (300 °C) exhibited good compressive behaviour with an optimum post weld isothermal holding time of 1 h and 45 min.

Alloy B electrode composition and B BT1 thermal cycle can therefore be used with preheat of 300 °C and post weld isothermal holding at the same temperature for about 2 h to achieve CFB weld microstructures.

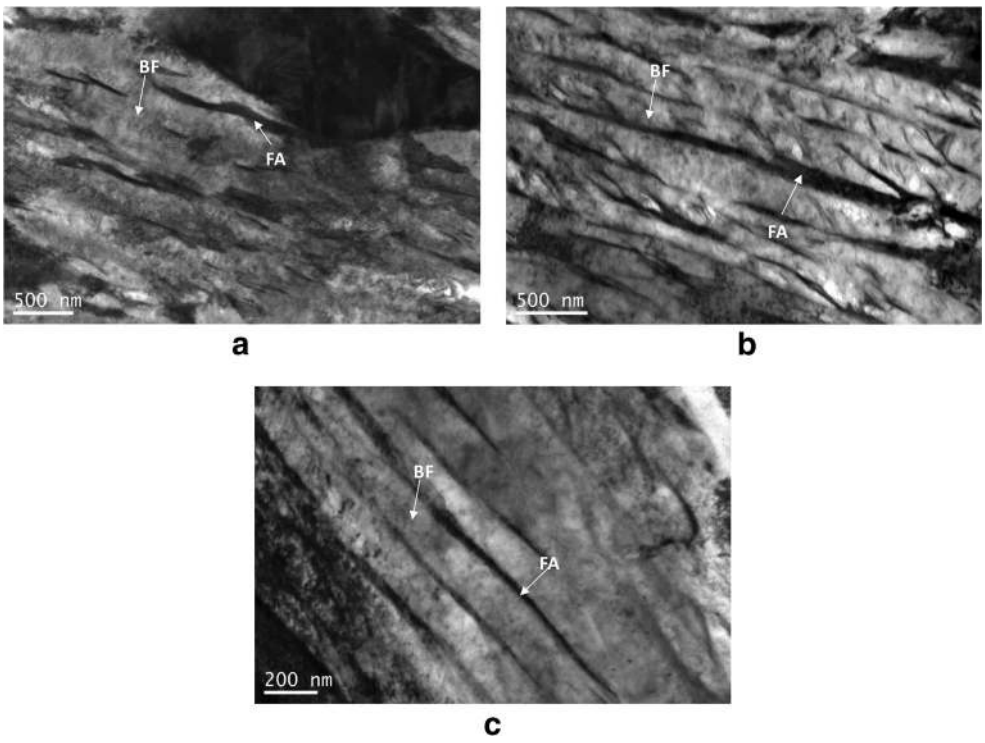

Fig. 22 TEM images of A BT1 (**a**), B BT1 (**b**), and C BT2 (**c**) welds. BF, bainitic ferrite; FA, filmy austenite

6 Conclusions

1. Electrode compositions required to stabilise carbide-free bainite and retained austenite containing microstructures can be designed with a combined thermodynamic calculations and experimental investigations.
2. Carbide-free bainite microstructures can be achieved with 0.85 volume fraction of bainitic ferrite and inter-lath retained austenite (RA) with alloy composition B of 0.375C-1.53Si-1.63Mn-0.17Ni-2.23Cr-0.19Mo (wt.%) and welding thermal cycle of B BT1 (a preheat of 300 °C and post weld holding at 300 °C for 2 h). It should be noted that this composition is identified to produce CFB weld microstructure under the assumption that dilution from base metal is neglected. In actual welds, electrode composition should be optimised by considering the dilution effects. Moreover, the prolonged preheating and post weld isothermal holding can also affect the base metal properties in real welds. Further investigation is required to ascertain the effect of preheating and post weld isothermal holding on the mechanical properties of the base metal during welding.
3. An increase in carbon content results in finer CFB structure; however, the stabilisation of blocky austenite with increased carbon can significantly affect the mechanical properties of the welds.
4. The methodology reported here to develop SMAW electrodes can also be used for developing electrodes for more productive FCAW process upon further investigation.

Funding The authors thank the Science and Engineering Research Board (SERB), Department of Science and Technology, Government of India, for funding Extra Mural Research (EMR) (grant EMR/2016/002755) for financially supporting this work.

References

1. Garcia-Mateo C, Caballero FG (2005) Design of carbide free low temperature ultra high strength bainitic steels. ISIJ Int 45:1736
2. Garcia-Mateo C, Caballero FG, Bhadeshia HKDH (2005) Mechanical properties of low temperature bainite. Mater Sci Forum 500-501:495–502
3. Garcia-Mateo C, Caballero FG, Sourmail T, Cornide J, Smanio V, Elvira R (2014) Composition design of nanocrystalline bainitic steels by diffusionless solid reaction. Met Mater Int 20(3):405–415
4. Caballero FG, Santofimia MJ, Capdevila C, García-Mateo C, de Andres CG (2006) Design of advanced bainitic steels by optimisation of TTT diagrams and T_0 curves. ISIJ Int 46(10):1479–1488
5. Caballero FG, Bhadeshia HKDH (2004) Very strong bainite. Curr Opinion Solid State Mater Sci 8:251–257
6. Bhadeshia HKDH (2016) Prevention of hydrogen embrittlement in steels. ISIJ Int 56:24–36
7. Szost BA, Vegter RH, Rivera-Diaz-del-Castillo PEJ (2013) Hydrogen-trapping mechanisms in nanostructured steels. Metall Mater Trans A 44A:4542–4550
8. Alkemade SJ (1996) The weld cracking susceptibility of high hardness armour steel. Australia: Defence Science and Technology Organization. p. 1–14 AR no. 009-659
9. Madhusudhan Reddy G, Mohandas T, Tagore GRN (1995) Weldability studies on high-strength low-alloy steel using austenitic stainless steel filler. J Mater Process Technol 49:213–228
10. Bhadeshia HKDH, Lord M, Svensso LE (2003) Silicon rich bainitic steel welds. Joining and welding solutions to industrial problems, JWRI, Osaka University, Osaka, pp 43–52
11. Fang K, Yang JG, Liu XS, Song KJ, Fang HY, Bhadeshia HKDH (2013) Regeneration technique for welding nanostructured bainite. Mater Des 50:38–43
12. Krishna murty N, Janaki ram GD, Murty BS, Reddy GM, Rao TJP (2014) Carbide-free bainitic weld metal: a new concept in welding of armor steels. Metall Mater Trans B Process Metall Mater Process Sci 45b:2327
13. Bhadeshia HKDH The nature, mechanism and properties of strong bainite. Proceedings of the 1st International Symposium on Steel Science (IS3–2007) the Iron and Steel Institute of Japan
14. Bhadeshia HKDH (2010) Nanostructured bainite. Proc R Soc A 466
15. Solimon M, Palkowski H (2007) Ultra-fine bainite structure in hypo-eutectoid steels. ISIJ Int 47(12):1703–1710
16. Garcia-mateo C, Caballero FG, Bhadeshia HKDH (2003) Acceleration of low-temperature bainite. ISIJ Int 43(11):1821–1825
17. Huang H, Sherif MY, Rivera-Dıaz-del-Castillo PEJ (2013) Combinatorial optimization of carbide-free bainitic nanostructures. Acta Mater 61:1639–1647
18. Andrews KW (1965) J Iron Steel Inst 203:721–727